

# Scaling-violation phenomena and fractality in the human posture control systems

Stefan Thurner,<sup>1,2</sup> Christian Mittermaier,<sup>3</sup> Rudolf Hanel<sup>4</sup> and Klaus Ehrenberger<sup>1</sup>

<sup>1</sup>*Klinik für HNO, Universität Wien, Austria*

<sup>2</sup>*Institut für Mathematik, NuHAG, Universität Wien, Austria*

<sup>3</sup>*Klinik für Physikalische Medizin, Universität Wien, Austria*

<sup>4</sup>*Institut für Theoretische Physik, Universität Wien, Austria*

By analyzing the movements of quiet standing persons by means of wavelet statistics, we observe multiple scaling regions in the underlying body dynamics. The use of the wavelet-variance function opens the possibility to relate scaling violations to different modes of posture control. We show that scaling behavior becomes close to perfect, when correctional movements are dominated by the vestibular system.

Keywords: balance system, wavelet analysis, scaling exponents,  $1/f$  noise, multifractal

PACS: 87.10.+e, 87.19.St, 87.19.Bp

## I. INTRODUCTION

Over the last years evidence has been compiled that many physiological systems and processes exhibit scaling laws in the corresponding time series [1], due to the existence of control mechanisms with a minimum degree of complexity. Irregularities in physiological processes may lead to scaling violations which recently have successfully been used to detect abnormalities of the underlying biological systems such as the human heart [2,3].

For some reason nature choose to let man walk upright. This has led, over time, to a highly complex balance system, which is not based on one single physical principle alone. Balance of a normal human being is the result of a most likely nonlinear [4] superposition of sensory signals originating from the vestibular, visual and somatosensory systems, which govern a cascade of muscular correctional movements in order to maintain an upright position, for an overview see e.g. [5]. The existence of three different mechanisms for maintaining balance provides the body with backup systems. If the vestibular system is severely damaged or not fully functioning, visual and somatosensory information will gain importance and take up for the loss.

Human posture can be quantified by measuring the displacement of the center of pressure under the feet of a quiet standing person, leading to time-varying trajectories Fig. 1. It is known in posturography that in case of damages of one component of the balance system certain characteristic frequency bands will change their relative weights, see e.g. [6]. Frequency bands provide a crude indicative of typical functional aberrations in the visual, vestibular, somatosensory and central nervous system. The visual system is linked to frequencies in the range of 0-0.1 Hz which dominate normal steady and undisturbed posture. Vestibular stress and disturbances will lead to enhanced frequencies in the 0.1-0.5 Hz band; frequencies between 0.5 and 1 Hz indicate somatosensory activity and postural reflexes mediated by the lower extremities. Finally, signs for malfunctions in the central nervous system usually correlate to high frequencies, i.e. 1 Hz and higher [6,7].

In this paper we provide first evidence that the different control mechanisms, at work at their characteristic time scales, lead to different scaling behavior in the center of pressure trajectories. By using a novel sensitive scaling measure based on wavelet statistics, we not only show that quiet standing is a correlated noise which has been observed before [8,9] but that in normal posture the mode of the control mechanism at work, is directly related to one of the multiple scaling regions with their characteristic scaling exponents. Scaling is found to be close to perfect (one single scaling exponent) in the case where visual and tactile senses are excluded, and the vestibular system plays the dominant role. This difference in scaling behavior could be used to directly quantify the relative importance of the vestibular system in relation to the entire human balance system. The wavelet measure is able to capture this scaling differences from standard posturography data on an individual basis. This suggests that the measure could be of clinical use in diagnostic of the functional quality of the different control mechanisms of human posture.

The paper is organized as follows: In Sect. II we review the concept of scaling statistics and conventional methods for its quantitative treatment. We further discuss a novel wavelet-variance function method. In Sect. III the experimental setup and the way of data acquisition are described. Results and a comparison of the different methods are presented in Sect. IV. Section V concludes with a discussion of the findings and their potential clinical usefulness.

## II. METHODS

To completely characterize processes from a stochastic point of view, the knowledge of all possible joint probabilities of the various events occurring in these processes is necessary. Fractal stochastic processes exhibit scaling in their statistics, which naturally lead to power-law behavior. Consider a statistic  $f$  which depends continuously on the scale  $x$  over which measurements are taken. Suppose the scale gets changed by a factor  $a$  and induces the statistics to get scaled by another factor  $g(a)$ , related to the factor but independent of the original scale:

$$f(ax) = g(a)f(x). \quad (1)$$

The only nontrivial solution to this scaling equation for real valued functions and arguments is

$$f(x) = bg(x) \quad \text{with} \quad g(x) = x^c, \quad (2)$$

for some constants  $b$  and  $c$ , e.g. [10,11]. The particular case of a fixed  $a$  admits a more general solution,  $g(x;a) = x^c \cos[2\pi \ln(x)/\ln(a)]$  [12].

### A. Scaling Measures

Over the years there have been developed a vast number of statistics to characterize stochastic processes, some which have already been applied to human posturography data. Maybe the most direct approach to quantify scaling is to use *two-point correlation functions* of the underlying (continuous or discrete) process  $x(t)$  (variance of  $\tau$ -increments):

$$K(\tau) = \langle [x(t+\tau) - x(t)]^2 \rangle_t \quad (3)$$

where  $\langle \cdot \rangle_t$  denotes the average over  $t$ . For processes of the kind of fractional Brownian motion the correlation  $K(\tau)$  scales as  $K(\tau) \sim \tau^{2C}$ . For  $C = 1/2$  the diffusion result is obtained (Brownian motion). This measure has been used recently to show that the dynamical process of quiet standing contains long term correlations, and thus can be interpreted as a correlated noise [13,8,9].

Another method frequently used to quantify scaling behavior of time series is to analyze the corresponding (discrete) *Fourier spectra*,

$$\tilde{X}(\omega) = \left| \sum_{k=1}^N x(k) e^{i2\pi(\omega-1)(n-1)/N} \right|^2 \propto \omega^S, \quad (4)$$

to determine the Fourier-scaling exponent  $S$ . Fourier analysis strongly depends on the stationarity of the underlying signals, which is often not the case for real world data. In particular posturography data contains drifts originating from slow correctional movements. It is common practice in time series analysis to apply Fourier methods after some sort of ‘detrending’ of the signals.

In the course of improving correlation measures, factors like the *Fano* and *Allan factor* have been proposed and applied widely for stochastic point processes [10]. Those factors are not necessarily limited to point processes, and can be used to obtain statistical information of time series. For an overview, especially for the relations of these factors to the power-spectral density, see [11]. The basic idea behind those and related measures is to compare sets of aggregated (over some time interval) events, rather than just looking at increment statistics as in the case of two-point correlation functions. As a further generalization of this the concept, the wavelet-variance function (WVF) has been introduced [2,3].

### B. Wavelet-variance function

Multiresolution wavelet analysis [14–18] has proved to be a mathematically clear and practical tool for analyzing signals at multiple scales, even in the presence of nonstationarities [19,20], which are obviously present in the center of pressure time series  $x$  and  $y$ , Fig. 1b. It was shown that wavelet statistics can be used to reveal scaling phenomena in natural systems in a more transparent way [2,21,3] than other methods frequently used.

In a first step we transform our time series into a (two dimensional) space of wavelet coefficients. Technically the coefficients are obtained by carrying out the discrete wavelet transform (DWT) [14] of  $x$ :

$$W_{m,n}^{\text{wav}}(x) = 2^{-m/2} \int_{-\infty}^{\infty} x(t) \psi(2^{-m}t - n) dt, \quad (5)$$

(same for  $y$ ) where the scale variable  $m$  and the translation variable  $n$  are integers. The discrete wavelet transform is evaluated at the points  $(m, n)$  in the scale–interval–number plane. Smaller scales correspond to more rapid variations and therefore to higher frequencies.

We have carried out this transformation using a broad range of orthonormal, compactly supported analyzing wavelets. Throughout the paper we present results for the Daubechies 10-tap wavelet. Similar results were obtained using Mallat and Haar wavelets. Orthogonality in the DWT provides that the information represented at a certain scale  $m$  is disjoint from the information at other scales. Because certain wavelets  $\psi$  have vanishing moments, polynomial trends in the signal are automatically eliminated in the process of wavelet transformation [18,20,19]. This is salutatory in the case of the time series  $x$  and  $y$ , as is evident from the trends apparent in Fig. 1b. Since the signal  $x(t)$  fluctuates in time, so too does the sequence of wavelet coefficients at any given scale, though its mean is zero since  $\int_{-\infty}^{\infty} \psi(t) dt = 0$ .

In [2] it was suggested to investigate the scaling behavior of the *statistics* of the wavelet coefficients at a particular scale of the signal of interest, resulting in the wavelet-variance function

$$\sigma_{\text{wav}}^2(m) = \frac{1}{N-1} \sum_{n=1}^N (W_{m,n}^{\text{wav}}(x) - \langle W_{m,n}^{\text{wav}}(x) \rangle_n)^2 \propto m^{2\Delta}, \quad (6)$$

where  $N$  is the number of wavelet coefficients at a given scale  $m$  ( $N = M/2^m$ , with  $M$  being the total number of sample points in the signal).  $\langle W_{m,n}^{\text{wav}}(x) \rangle_n$  denotes the mean taken at a given scale. For reasonably long signals this quantity will be close to zero and can be neglected for practical purposes.

It is not straight forward to relate the wavelet-variance scaling exponent  $\Delta$  to the Fourier-scaling coefficient  $S$ . The exponent  $\Delta$  may to some extent depend on the choice of the type of wavelets. However, the Allan factor when multiplied by the mean, can be seen as a special case of the WVF if the Haar wavelet is taken, and a relation to the Fourier-scaling exponent can be established [11]. Later in this work we present an empirical relation based on fractal Gaussian noise (FGN) surrogate data and on the Daubechies 10-tap wavelets.

### III. DATA AND EXPERIMENTAL SETUP

For measuring the movements of an upright standing person, the person was placed on a standard posturography plate [22], which is sensitive to weight shifts. Data was gathered on 37 healthy subjects (Age:  $31.7 \pm 6.8$  years, Weight:  $66.3 \pm 12.2$  kg, Height:  $173.0 \pm 8.9$  cm, Sex: 19 females, 18 males), who had no history of dizziness, have never suffered any leg injuries, nor were taking any form of medication before the measurements. The sample contains no subject with musculo-skeletal, neurologic or vestibular disorder. The measurements were taken with the subjects looking in the forward direction, wearing no shoes and no long pants or skirts, to avoid tactile feedback loops along the legs. Individual tests lasted for 20 seconds as is a typical clinical posturography standard, points were sampled at a rate of 50 Hz. The reason for keeping the measurements short is to reduce the probability that the subject would change its standing strategy (toe or hip strategy) within a single measurement. Each subject was measured three times to ensure consistency.

The output of the plate is the trajectory of the center of gravity projected onto the  $xy$  plane, Fig. 1a. The actual measured  $x$  and  $y$  trajectories have been shifted by their mean,  $x = x_{\text{measured}} - \langle x_{\text{measured}} \rangle_t$  (same for  $y$ ). For the complete knowledge of a dynamical system the time series of the momenta are also needed. We obtain an estimate of these by taking time derivatives (first differences) of the  $x$  and  $y$  trajectories and denote them by  $v_x = \frac{d}{dt} x$  and  $v_y = \frac{d}{dt} y$ , respectively, Fig. 1c. All further analysis has been carried out on these position and ‘velocity’ trajectories. Figure 1d shows the phase-space plot of the  $y$ -component for the same data.

To estimate systematic measurement errors, we placed a mass of 75 kg on the platform. The resulting trajectories, which relate to vibrations of the floor and the measuring equipment, were confined to elongations of less than 0.02 cm.

#### A. Experiments

To be able to study different modes of posture control we performed four types of measurements. In the first type the subject was asked to stand still with eyes open (eo). The resulting movements are the bodily responses to a mixture of visual, somatosensory and vestibular input.

In the second test the subjects were asked to close their eyes (ec), and were additionally provided darkened swimming glasses, so that no visual input could influence posture control.

The third and fourth test were done on a foot plate that could sway in the forward-backward ( $y$ ) direction. We refer to this as the eyes-open-moving plate (eomp) and the eyes-closed-moving plate (ecmp) tests. The experimental design of these tests was to reduce somatosensory effects originating in pressure sensors of the foot. Note that in this setup the pressure on toes and heel is kept constant during the measurement due to the moving plate: Whenever force is applied by the toes the plate moves down in the front, as it will move down in the back whenever force is exerted by the heel. While in the eomp test, visual and vestibular systems are active, the resulting movements in the  $y$ -direction in the ecmp test will be dominated by the vestibular system alone.

#### IV. RESULTS

In order to relate the wavelet-scaling exponent  $\Delta$  to the more familiar Fourier-scaling exponent  $S$ , we generated fractal Gaussian noise (FGN) time series, of definite Fourier-scaling exponent  $\alpha_{\text{theory}}$ . From those time series we computed the Fourier-scaling exponent  $S$ , which should be the same as  $\alpha_{\text{theory}}$ , and the wavelet-scaling exponent  $\Delta$ . The results for the Daubechies 10-tap wavelets are given in Tab. I. A linear fit yields an estimate of the relation of the two scaling measures:

$$\Delta = -(0.019 + 0.311 S) \sim -S/3. \quad (7)$$

For each  $\alpha_{\text{theory}}$  we generated 50 FGN time series, and averaged over the extracted exponents.

Figures 2a and 2b show  $\sigma_{\text{wav}}(x)$  and  $\sigma_{\text{wav}}(y)$  as a function of scale  $m$  for the eo and ecmp tests of a representative subject. Time scales  $m$  correspond to data segments of a length of  $\frac{2^m}{50}$  seconds<sup>1</sup>. It is seen that for the eo-case the curve is a straight line from scale two on. For the small scales, the slope - the wavelet-scaling exponent - denoted by  $\Delta_S(x)$  (scale 1 to 2), is clearly less than the slopes at larger scales  $\Delta_L(x)$ , indicating the onset of white noise<sup>2</sup> in the high frequency region, i.e. the small scale region. For the ecmp situation, no such scaling violation is observed, and  $\Delta_S \sim \Delta_L$ . We have checked that this finding is independent of whether discrete or continuous wavelets are used, and that it is reasonable to extract the scaling exponent  $\Delta_S$  from the smallest 2 scales only in the discrete case. For very large (VL) scales ( $m = 6 - 10$ ) we find a significant decrease in the corresponding scaling exponent  $\Delta_{VL}$  compared to  $\Delta_S$  and  $\Delta_L$ . However at those large scales for our relatively short data sets ( $M = 1000$ ) statistics becomes sparse and the estimates for  $\sigma_{\text{wav}}^2(m > 5)$  rather unreliable.

These observations lead us to consider an index quantifying the degree of scaling violation, determined by the quotient of the wavelet-scaling exponents in large ( $\Delta_L$ ) and small ( $\Delta_S$ ) scale regions:  $\Delta_{\text{sv}} = \Delta_L/\Delta_S$ . In Fig. 3a the mean values over the whole sample are shown for all of the measurements (37 subjects à 3 times). It is clearly observable that the scaling violation measure  $\Delta_{\text{sv}}$  approaches 1 when suppressing visual and tactile control (ecmp), and that it nicely distinguishes between the modes of posture control. In Fig. 4a we present  $\Delta_{\text{sv}}(y)$  for all subjects for the eo and ecmp-tests. The reduction of  $\Delta_{\text{sv}}$  from the eo-case to the ecmp-case is apparent. This effect is less pronounced in the  $x$ -direction in which the plate is stable. The scatter plot in the velocity-scaling-position-scaling-violation plane also suggests a slight positive correlation of velocity-scaling with the index of scaling violation.

We found that the two-point correlation function used on the same data set shows scaling differences similar to those reported in [8,9], but that it is not sensitive enough to clearly distinguish between different modes of posture control. For comparison we show the quotient of the corresponding high ( $C_{\text{High}}$ ) and low ( $C_{\text{Low}}$ ) scaling regions  $C_{\text{High}}/C_{\text{Low}}(y)$  in Fig. 3b for the same measurements. We were able to reproduce within errors the two-point correlation scaling values in the high and medium frequency domain of [8]. Our results are  $C_{\text{Low}}(y)_{\text{eo}} = 0.71 \pm 0.07$ , and  $C_{\text{High}}(y)_{\text{eo}} = 0.20 \pm 0.19$ . Also the critical time where the scaling regimes of  $C$  change could be confirmed to be somewhat less than a second, which corresponds to the change of wavelet-scaling regimes  $\Delta_L(y)_{\text{eo}} = 0.85 \pm 0.1$  to  $\Delta_{VL}(y)_{\text{eo}} = 0.25 \pm 0.27$  at scale  $m = 6$  (1.28 sec), see Tab. II. As for the quotient  $C_{\text{High}}/C_{\text{Low}}$  also  $\Delta_{VL}/\Delta_L$  is found to be not well suited for a separation of the standing modes, especially not on an individual basis. Note here

---

<sup>1</sup>The smallest reasonable scale for the given sampling rate of 50 Hz is thus  $m = 1$  or 1/25 sec. The reason why we did not consider smaller scales is most clearly seen for the (discrete) Haar wavelet: at scale  $m = 1$ , only two sample points will be in the support of the wavelet. At a smaller time scale ( $m = 0$ ),  $\sigma_{\text{wav}}^2(0)$  would be identical to the variance of the signal.

<sup>2</sup>a slope of zero is equivalent to white noise

that the wavelet-scaling regimes from  $\Delta_S$  to  $\Delta_L$ , which are sensitive to posture control, change at scales  $m = 2$  and  $3$ , corresponding to about  $1/10^{\text{th}}$  of a second.

Our standard deviation of  $C_{High}(y)$  is considerably larger than reported in [8], which is explained by the fact that the data length there is 4.5 times larger (90 sec) than the data used here. For our relatively short data segments it was not possible to reliably estimate the third scaling region for time scales larger than 10 seconds for all of the described methods. In this region scaling vanishes due to the limited extend of motion [9].

Values for the various scaling exponents and the scaling violation quotients are gathered in Tab. II together with the kurtosis and skewness of the increment processes  $v(y)$ . The latter indicate almost Gaussian distributions for the steady plate case which changes clearly towards leptocurtic distributions in the moving-plate scenario. The leptocurticity reflects the existence of periods of fast correctional movements followed by periods of relatively quiet standing in the moving plate scenarios. In financial time series analysis this behavior in dynamics is referred to as volatility clustering.

We continue by analyzing scaling behavior of the increment (‘velocity’) processes. In Figs. 2c and 2d,  $\sigma_{\text{wav}}(v_x)$  and  $\sigma_{\text{wav}}(v_y)$  demonstrate that in the eo-case the wavelet-scaling exponents are generally small for the corresponding velocities, which means little correlation or structure. For the ecmp-case the wavelet exponent associated to  $v_y$ ,  $\Delta_L(v_y)$ , is drastically enhanced, while  $\sigma_{\text{wav}}(v_x)$  is compatible with the eo-case, as expected. This behavior was encountered in all subjects of the sample of 37 healthy test persons, as can be inferred from Fig. 4a.

To compare the wavelet-variance method to conventional Fourier methods, we extracted Fourier-scaling exponents  $S$  from the data. Since the original signals  $x$  and  $y$  are nonstationary, doubts on the reliability on a straight forward use of power spectra are justified. However, already naive Fourier spectra, after windowing, show typical  $1/f$  behavior and it is possible to observe different scaling exponents in most subjects in the low ( $S_{Low}(y)$ ) and high frequency regions ( $S_{High}(y)$ ). The data does not allow for a stable estimate of the degree of the corresponding scaling violation, since the inter- and intra-subject variance are high, which is reflected in the large standard deviations in the corresponding scaling violation quotient  $S_{Low}(y)/S_{High}(y)$  in Tab. II. The Fourier-scaling exponents for  $S_{Low}(y)$  and  $S_{High}(y)$  were obtained from fits in the power spectrum in the region of 1.45 Hz - 12.45 Hz and 12.45 Hz - 25 Hz respectively. We note here that within errors the relation given in eq. (7) still holds approximately for the experimental data  $\Delta_S$  vs.  $S_{High}$  and  $\Delta_L$  vs.  $S_{Low}$  (large scales correspond to low frequencies). This could be a sign that the two different scaling regions could be successfully modeled with FGN models. However since errors are large for the estimates of  $S_{High}$  and  $S_{Low}$ , one should be careful in interpreting this result in terms of the nature of the underlying processes at the different scaling regions.

No problem with nonstationarity will arise when the derivatives  $v_x$  and  $v_y$  are used, and clearly  $1/f$  behavior is observed. The corresponding Fourier-scaling exponents  $S(v_y)$  for the individual subjects for two tests are gathered in Fig. 4b. It is clearly seen that the two tests separate in this variable,  $S$  drops by a factor of 3 on average. In both tests a slight decrease of the scaling exponent on age is observable.

We have computed cross correlation functions of  $x$ ,  $y$ ,  $v_x$  and  $v_y$  components. We could not find a significant dependence of one on the other for all measurements, and could such exclude torque effects in quiet standing in healthy subjects.

Additionally we have computed the boxcounting dimension  $D_{bc}$  of the graphs in Fig. 1a for all subjects. The largest box was taken to be  $6 \times 6$  cm for all measurements. The results are given in Fig. 4c. It is remarkable that in this variable, which is a measure of the *static* geometry of the posture trajectory, separation of the different tests occurs, Tab. II.

## V. DISCUSSION

All the conventional scaling measures used in this work were able to confirm that human posture is indeed a correlated process, and indicate that different scaling regions are present (multifractal). The wavelet-variance function method proves to exhibit these scaling violations in a very precise way so that it becomes possible to relate the different control mechanisms to different scaling exponents on an individual basis. We show that this is even possible on very short (standard) posturography data, clearly outperforming the other methods.

In particular we demonstrated that dominance of the vestibular system shows close to perfect scaling phenomena in the position time series. When visual and tactile input information are superimposed on the vestibular system, scaling violations occur, pointing of course at a nonlinear interplay of the underlying systems and their relevant characteristic time scales. For the ‘velocity’ time series the effect is even more pronounced since the pure vestibular system shows clear scaling, which breaks down almost completely for the superposition cases.

The findings presented here might bear a potential for practical use: since the scaling exponents and scaling violation measures can be considered as tools which measure the relative importance of the vestibular system in comparison

with the visual and somatosensory systems, it seems sensible that they provide a key for a *direct* measurement of the intactness of the vestibular system. Clinical practice today is to measure this intactness of the vestibular system by thermally disturbing it and measuring the resulting eye movements. A particular interesting subject will be an analysis, along the lines presented here, of sway data of patients with dizziness, which often goes hand in hand with vestibular stress or malfunction.

We found first evidence that some scaling measures are age dependent. It might be possible to quantitatively relate a loss of complexity in the posture control systems of the aging human to changes in scaling measures.

---

- [1] J.B. Bassingthwaite, L.S. Liebovitch and B.J. West, *Fractal Physiology* (Oxford Univ. Press, New York, 1994).
- [2] S. Thurner, M.C. Feurstein and M.C. Teich, *Phys. Rev. Lett.* **80**, 1544-1547 (1998).
- [3] S. Thurner, M.C. Feurstein, S.B. Lowen and M.C. Teich, *Phys. Rev. Lett.* **81**, 5688-5691 (1998).
- [4] K.M. Newell, R.E.A. Van Emmerik, D. Lee and R.L. Sprague, *Gait and Posture* **4**, 225-230 (1993).
- [5] J. Massion, *Current Opinion in Neurobiology* **4**, 877-887 (1994).
- [6] U. Oppenheim, R. Kohen-Raz, D. Alex, A. Kohen-Raz and A. Azarya, *Diabetes Care* **22**, 328-332 (1999).
- [7] R. Kohen-Raz, private communication.
- [8] J.J. Collins and C.J. DeLuca, *Phys. Rev. Lett.* **73** 764-767 (1994).
- [9] C.C. Chow and J.J. Collins, *Phys. Rev. E* **52** 907-912 (1995).
- [10] S.B. Lowen and M.C. Teich, *Fractals* **3**, 183-210 (1995).
- [11] S. Thurner, S.B. Lowen, M.C. Feurstein, C. Heneghan, H.G. Feichtinger and M.C. Teich, *Fractals* **5**, 565-595 (1997).
- [12] M.F. Shlesinger and B.J. West, *Phys. Rev. Lett* **67**, 2106-2108 (1991).
- [13] J.J. Collins and C.J. De Luca, *Exp. Brain Res.* **95**, 308-318 (1993).
- [14] I. Daubechies, *Ten Lectures on Wavelets* (Society for Industrial and Applied Mathematics, Philadelphia, PA, 1992).
- [15] S. Mallat, *Trans. Amer. Math. Soc.* **315**, 69-88 (1989).
- [16] Y. Meyer, "Ondelettes, fonctions splines et analyses graduées," Lectures given at the University of Torino, Italy (1986).
- [17] A. Aldroubi and M. Unser eds., *Wavelets in Medicine and Biology* (CRC Press, Boca Raton, FL, 1996).
- [18] A. Arneodo, G. Grasseau and M. Holschneider, *Phys. Rev. Lett.* **61**, 2281-2284 (1988).
- [19] P. Abry and P. Flandrin, in *Wavelets in Medicine and Biology* (CRC Press, Boca Raton, FL, 1996), pp. 413-437.
- [20] M.C. Teich, C. Heneghan, S.B. Lowen and R.G. Turcott, in *Wavelets in Medicine and Biology* (CRC Press, Boca Raton, FL, 1996), pp. 383-412.
- [21] A. Marrone, A.D. Polosa, G. Scioscia, S. Stramaglia, and A. Zenzola, *Phys. Rev. E.* **60**, 1088-1091 (1999).
- [22] Data was gathered with a "Pro Balance Master" (Neurocom Intl. Inc.).

$\alpha_{\text{theory}}$	$-S$	$\Delta$
0.5	0.51(0.06)	0.14(0.02)
1.0	0.96(0.07)	0.27(0.03)
1.5	1.50(0.07)	0.45(0.02)
2.0	2.00(0.06)	0.64(0.03)
2.5	2.52(0.06)	0.73(0.04)

TABLE I. Relation of Fourier-scaling exponent and the wavelet-variance exponent obtained from fractal Gaussian noise surrogate data of definite Fourier-scaling exponent  $\alpha_{\text{theory}}$ . To match experimental data the noise sequences contained 1000 samples each, averages of the exponents were taken over 50 sequences per  $\alpha_{\text{theory}}$ . The numbers in brackets are standard deviations.

	eo	ec	eomp	ecmp
$\Delta_L/\Delta_S(y)$	1.55(0.73)	1.46(0.66)	1.17(0.46)	1.02(0.41)
$\Delta_S(y)$	0.55(0.19)	0.62(0.21)	0.76(0.22)	0.91(0.26)
$\Delta_L(y)$	0.85(0.10)	0.91(0.10)	0.89(0.10)	0.92(0.11)
$\Delta_{VL}(y)$	0.25(0.27)	0.22(0.26)	0.28(0.25)	0.34(0.28)
$C_{Low}/C_{High}(y)$	3.67(4.00)	4.02(8.96)	3.07(2.00)	3.34(3.26)
$C_{Low}(y)$	0.71(0.07)	0.75(0.07)	0.71(0.06)	0.70(0.07)
$C_{High}(y)$	0.20(0.19)	0.19(0.25)	0.23(0.16)	0.21(0.18)
$S_{Low}(y)/S_{High}(y)$	4.97(8.42)	4.20(5.57)	2.35(1.84)	1.46(0.86)
$S_{Low}(y)$	-2.55(0.52)	-3.05(0.57)	-3.42(0.49)	-3.85(0.42)
$S_{High}(y)$	-0.51(0.77)	-0.73(0.83)	-1.46(0.94)	-2.64(1.28)
$S(y)$	-2.06(0.21)	-2.24(0.30)	-2.35(0.38)	-2.59(0.50)
$S(d/dt y)$	-0.43(0.23)	-0.74(0.28)	-1.08(0.28)	-1.50(0.21)
$D_{bc}$	0.67(0.16)	0.79(0.17)	1.00(0.18)	1.35(0.14)
kurtosis( $d/dt y$ )	3.49(1.67)	3.70(0.97)	5.34(2.42)	4.91(2.25)
skewness( $d/dt y$ )	0.040(0.198)	0.011(0.225)	0.060(0.424)	0.036(0.394)

TABLE II. Various scaling measures and kurtosis and skewness of the increment processes for the four different tests performed (eyes open (eo), eyes closed (ec), eyes-open–moving plate (eomp) and eyes-closed–moving plate (ecmp)). The value in bracket is the standard deviation over all measurements (3 per subject). Fits for  $S(y)$  and  $S(d/dt y)$  have been taken over the whole frequency range.

FIG. 1. Movement of the center of gravity projected on the  $xy$ -plane (a) for open eyes, stable plate. The time evolution of the motion for the  $x$  and  $y$  components is shown in (b). The time derivatives represent momentary ‘velocity’ (c). Whereas positions are clearly nonstationary for the 20 seconds time intervals, velocities are. (d) Phase-space diagram for the  $y$ -component. The form of the phase-space trajectory reminds on the Duffing oscillator with randomized phases. For clarity the plot has been smoothed by moving averages of block-size 4.

FIG. 2. Wavelet scaling exponents for the eyes open (eo), (left column) and the eyes-closed–moving plate (ecmp), (right) test. For the position data  $x$  and  $y$  (top line) scaling violation in eo is obvious for low scales. This violation is absent in ecmp. In the velocity data  $v_x$  and  $v_y$  scaling is generally low in eo, but becomes strong in the  $y$  component of ecmp.

FIG. 3. Comparison of the wavelet-scaling-invariance  $\Delta_L/\Delta_S(y)$  measure (a) and the corresponding correlation quotient  $C_{High}/C_{Low}(y)$  (b). In the latter there is no difference detectable in the mode of posture control. eo, ec, eomp and ecmp refer to the eyes open, eyes closed, eyes-open–moving plate and eyes-closed–moving plate tests respectively. The errorbars indicate mean standard errors.

FIG. 4. Scaling measures for the whole sample of 37 healthy persons. (a) velocity-scaling–position-scaling-violation plot. The scaling-violation measure  $\Delta_L/\Delta_S(y)$  is grouped around one for the eyes-closed–moving (ecmp) case, while it is larger for the eyes open test (eo). The wavelet-scaling exponent in  $v_y$  is significantly larger for the ecmp than for eo. Moreover a slight positive correlation of velocity-scaling with position-scaling-violation is observable. (b) Fourier-scaling exponents for velocities for all individuals ordered by age (left - young, right - old). (d) Box counting dimension  $D_{bc}$  for the same individuals. The symbols denote the means of the three identical measurements, the errorbars are the corresponding mean standard errors.



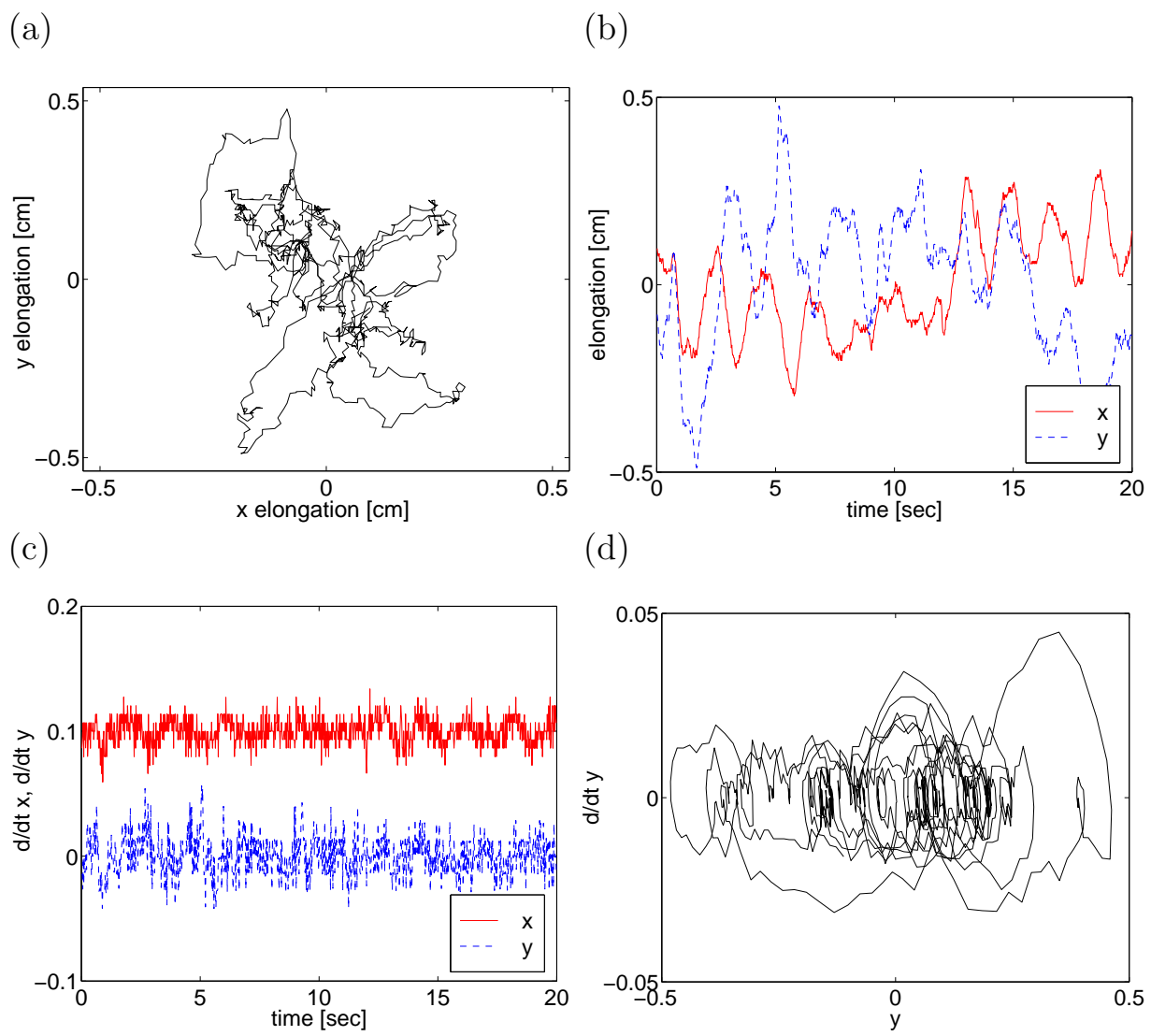


FIG. 1

eo

ecmp

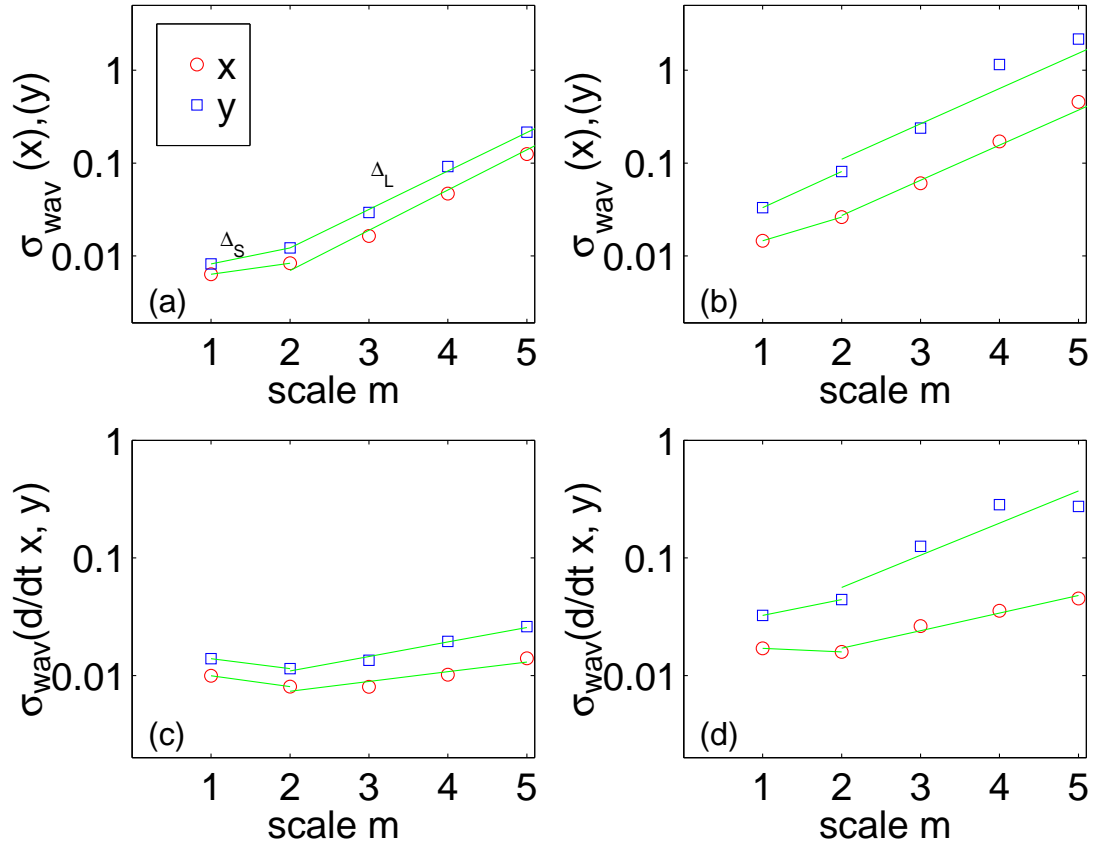


FIG. 2

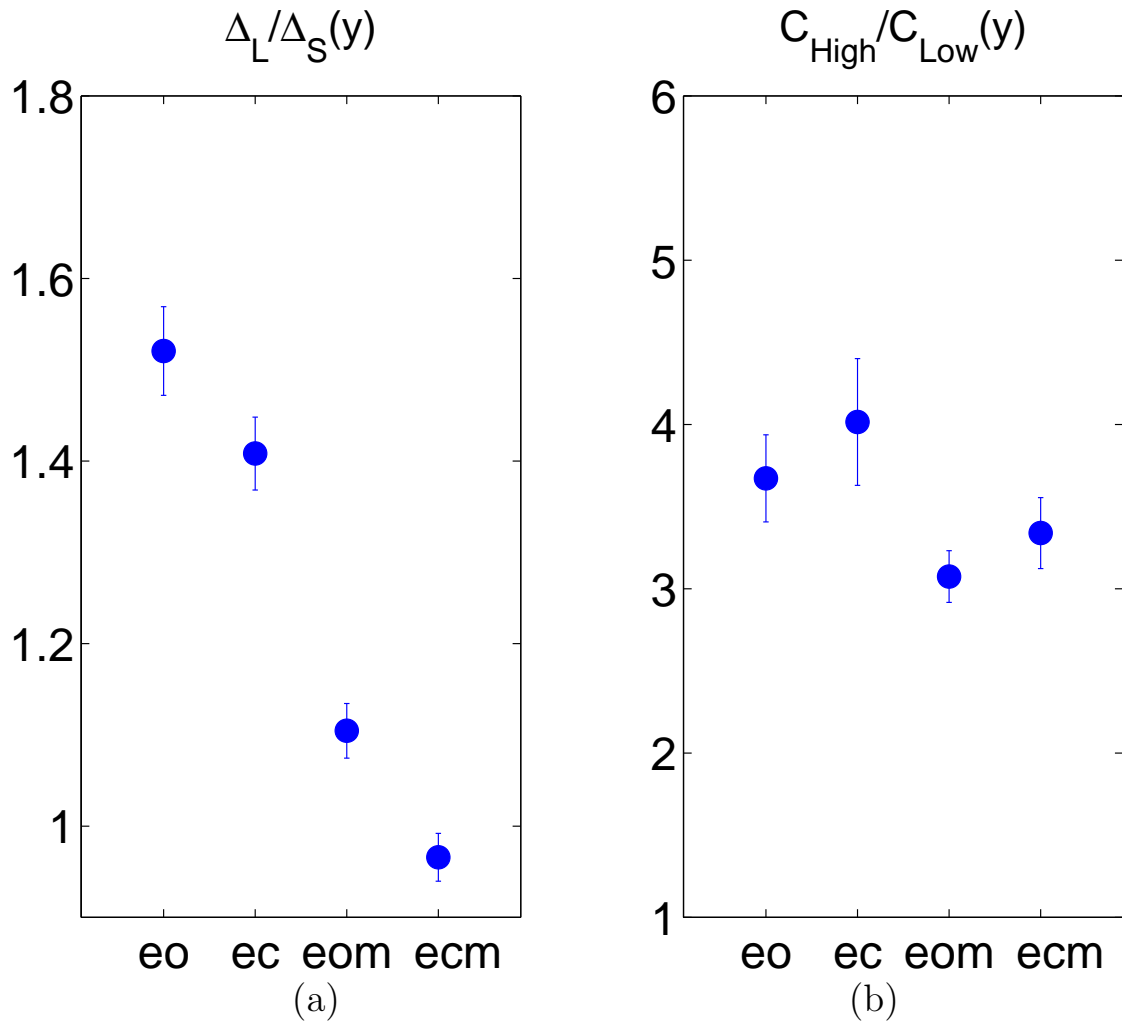
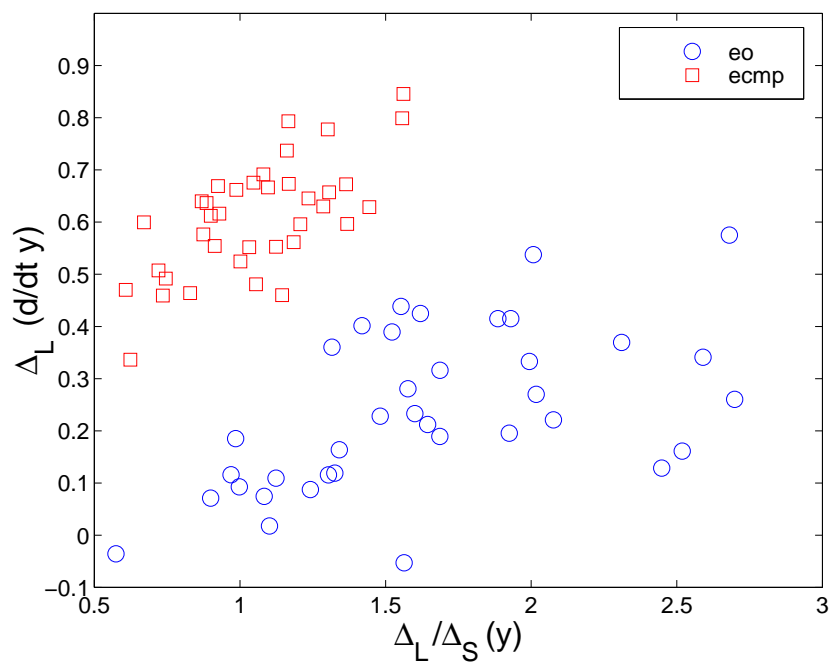


FIG. 3

(a)



(b)

(c)

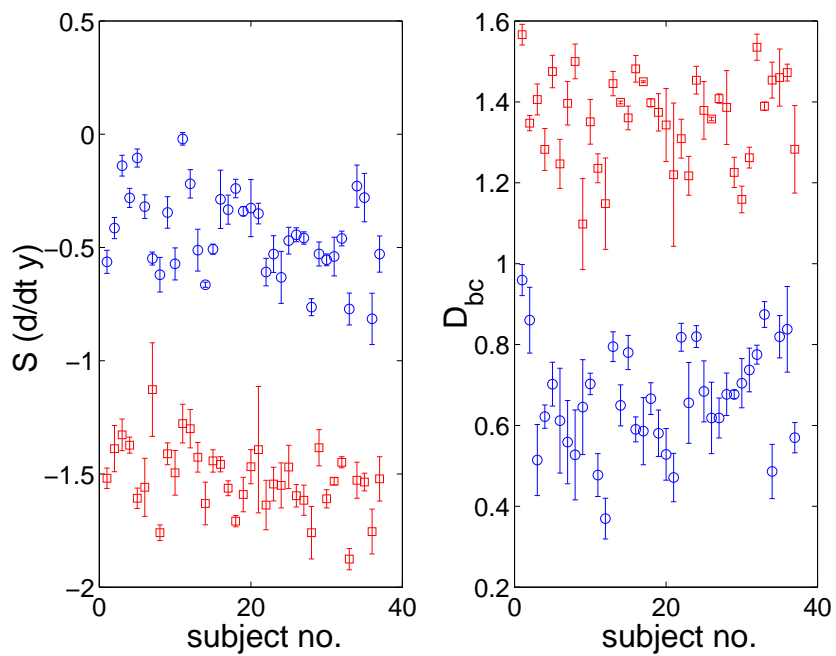


FIG. 4